Forward Looking Sonar Data Simulation through Tube Tracing

Didier Guériot and Christophe Sintes
Institut TELECOM ; TELECOM Bretagne
Technopôle Brest-Iroise, CS 83818, 29238 Brest Cedex 3, France
{didier.gueriot, christophe.sintes}@telecom-bretagne.eu

***Abstract*—Simulating realistic sonar data is crucial for tuning detection and classification algorithms according to environment and acquisition characteristics. Moreover, robustness of performances estimation and prediction applications can be greatly enhanced as soon as such a simulation tool provides both a modular underwater world representation (multiple sensors, environments and acquisition conditions) and a selection of several computational engines (ray theory, parabolic equation, . . .). Therefore, we developed such a framework for simulators, allowing both scene design and computational engine choice. Within it, two engines (one for rays, one for tubes) has been successfully implemented and realistic simulations obtained, as shown in the presented simulated sonar images. This paper introduces the simulation of a new imaging sensor (DIDSON acoustic camera) showing the extensibility of the proposed framework while providing realistic and specific front-looking simulated images. Moreover, in order to bypass the scene resolution given by the facet sizes, some georeferenced perturbations are introduced in order to model sub-facet behaviors and produce more realistic responses from the scene with micro and macro textures on the output images.**

***Index Terms*—Acoustic propagation, sonar framework simulation, sidescan sonar, interferometry, tube modeling, ray tracing**

I. Introduction

Due to operational constraints for underwater data acquisition, simulating realistic sonar data, like images and swath bathymetry profiles, is crucial for designing/tuning detection and classification algorithms according to sensors settings and sea-bottom nature and topography. Moreover, the robustness of any performances estimation or prediction can be greatly enhanced, as soon as such a simulation tool provides a modular and flexible underwater world representation (multiple sensors, environments and acquisition conditions). However, a second modularity axis is required as different computational engines may be used depending on simulation cases (ray theory, normal mode or parabolic equation, all solving the Helmholtz equation with specific approximations). Therefore, we developed such a framework for simulators, allowing both scene design and computational engine choice.

In the proposed approach, the virtual environment gathers fractal simulated or real elevation maps for sea-ground truth, sets of natural or manufactured bottom-laying items and seabed textures resulting from adequate spatial layouts of ground resolution cells. Moreover, taking into account carrier trajectory and attitude along time warrants multi-sensor realistic outputs [1].

Coming with this framework, two computational engines have also been developed, both aiming at rendering data similar to what real sensors provide in a natural context. Thus, the first one relies on acoustical ray tracing techniques tailored to consider specific underwater propagation properties while the second one, built on the top of the first, launches acoustic tubes in order to take into account volume interaction between the acoustic wave and the scene. Indeed, while the ray tracing engine offers a very nice rendering, the new proposed tube approach introduces a volume characterization of the insonified solid angle allowing an exhaustive description of the energy interacting with the scene and collected by the receiving sonar.

After presenting the key features of the simulator framework, this paper introduces a new simulated sensor (a DIDSON acoustic camera) within this framework. This introduction takes benefit from the existing propagation engines and adds a new sensor component which deals with this sensor specific behavior, highlighting the framework extensibility. Finally, two classes of georeferenced perturbations are proposed to take into account phenomena resulting from scene features smaller than object facet size or individual DTM cells coverage.

II. A multi-sensor simulator framework with engine plug-ins

A. Simulation environment & software components

The main goal of this simulation framework is to propose a common software environment for developing modular simulation tools.

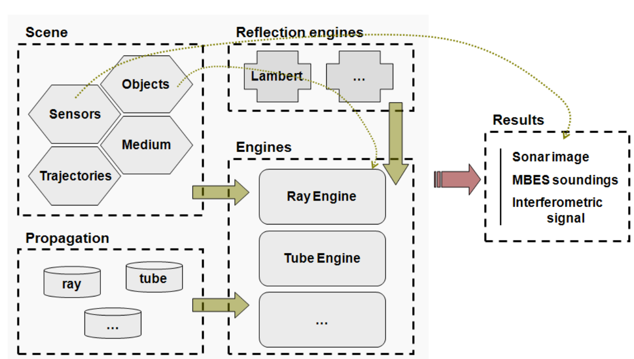

Fig. 1. Framework main software components

The keyword *modular* stands for both the simulation objects describing an underwater scene and the algorithms developed to deal with acoustic propagation and object interactions (reflection, refraction, . . .). Thus, the user picks among several families of components to tune its simulation environment. As shown in Figure 1, some of these software components are relative to static properties of the underwater scene while others are meant to represent dynamic phenomena.

The *scene* components family gathers all the objects (wrecks, containers, sea bottom elevation maps, . . .) belonging to the underwater environment, with their geometric descriptions either using mathematical definitions or through lists of facets. It also includes all the characteristics of the propagation media (sound velocity profile, . . .), the list of sensors involved in the simulation with their intrinsic properties and their dynamic behaviors (trajectories, attitudes, . . .).

The *propagation* package keeps all the models available for simulating acoustic wave propagation within a medium, while all the engines from the *engine* package rely on both a scene description and a propagation model to propose a full acoustic simulation. The engine main goal is to generate a propagation history from the transmitting to the receiving sensor, gathering along the propagation path, all the interactions between the acoustic wave and the scene elements. As shown in next sections, preserving such a propagation history allows each receiving sensor to aggregate all the incoming contributions to produce its specific sonar simulated data.

B. The Tube Engine

Within the global framework presented in the previous section, two engines have been developed in order to validate the required computational modularity. These first two engines basically rely on a ray approach to model the acoustic field propagation: the first considers an acoustic wave as a series of rays while the second uses these rays as support for a volume description of the insonified area. Results from the ray-only engine shows promising results [2]. However, the discrete modeling of the insonified volume brings various artifacts that can be avoided with a full tube engine that describes the volume between the rays [3]. The next lines will explain the basic behavior of such an engine in order to introduce later the new DIDSON sensor.

1) Tube engine algorithm principles: This engine represents acoustic wave propagation as a series of rays always orthogonal to the current local wave front. The solid angular range of such a wave, also called *sector*, depends on the aperture properties of the simulated antenna. Within this sector, tubes are built on the top of neighboring rays using four of them as borders, as shown in Figure 2. The intersection between a tube and a scene element defines a tube footprint. If this footprint is totally included in one facet of an element, it becomes an elementary footprint E_C.

With these definitions, the basic tube engine algorithm consists in a 3-step processing for each sector, as illustrated in Figure 3:

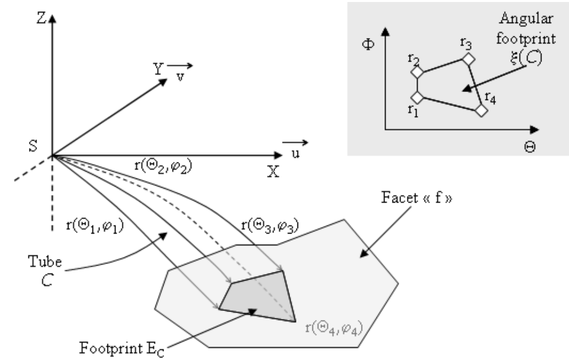

Fig. 2. Tube tracing mechanism and scene interaction through tube footprints

1) The transmitting sector S_1, defined by the Tx sensor properties, is split as long as it contains non-elementary tubes.
2) The same splitting process is performed for the receiving Rx sensor (sector S_2).
3) For each intersection between an elementary Rx tube and an elementary Tx tube, the corresponding footprint is computed allowing for the receiver to properly aggregate the transmitter contribution after its interaction with the intersected facet.

In case of multiple paths simulations, all the footprints belonging to a facet are gathered in order for this facet to become a new transmitter. The amount of levels in this recursive loop defines the number of multiple paths to consider.

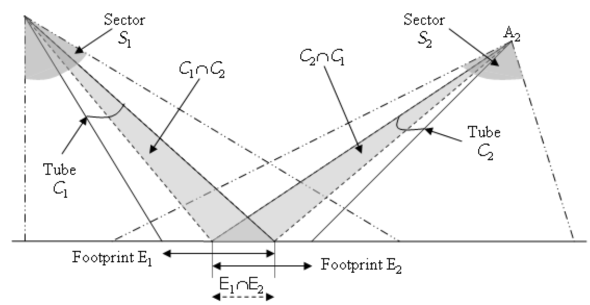

Fig. 3. Tube acoustic propagation from Tx sensor (sector S_1) to Rx sensor (sector S_2) through intersecting footprints

The strong key feature of this algorithm is to independently compute the full acoustic wave propagation history so that each receiving sensor uses this history to output data. Thus, in this paper, starting from the generic computed propagation history, several sensor output will be exhibited according to their sensor-specific aggregation algorithms.

C. Simulation results

Two experiments have been conducted in order to show the capabilities of the simulator either for imaging complex objects or elevation described sea bottoms. For each experiment a specific scene has been built. The first scene consists in an oil well head lying on a flat sandy bottom.

The oil well head geometry comes from a Wavefront file giving its edges and vertices. The second scene only contains a Digital Terrain Model built from multibeam echosounder bathymetric measurements collected for the "Shallow Survey '99" conference [4] in the Sydney harbor. This DTM used as ground truth for the simulation, has been built from the RESON 8101 bathymetry data, after appropriate calibration and georeferencing [5].

Each scene has been surveyed twice, using a sidescan sonar and then a multibeam echosounder. Images and soundings from these simulations follow.

1) Simulating sidescan sonar:

a) Aggregation principles: As illustrated in Figure 3, the Rx sector is split into Rx elementary tubes having a specific footprint into the scene, corresponding to the intersection between this Rx tube and the Tx sector inside a unique facet. The geometrical configuration and properties of this facet characterize the energy backscattered through each tube. When arriving on the Rx sensor, this temporal backscattered energy is sampled according to the sensor sampling frequency to fill up the corresponding pixels in the output image. Processing all the Rx elementary tubes completes the full image, involving a full energy preservation from the Rx sensor point of view.

b) Results: High resolution simulated sonar images have been produced by our simulator when using this tube engine and a *virtual* sidescan sonar to perform the acoustic data collection.

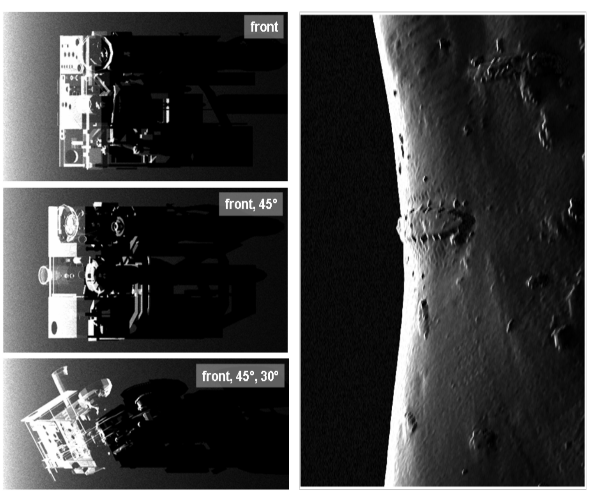

(a) Oil well head (b) Sydney harbor

Fig. 4. Sidescan simulations on the two reference scenes

Figure 4 presents such simulated images on the two reference scenes. They illustrate the capabilities of the simulator to perform well on either localized complex objects (here, the oil well head) or real sea bottom elevation models. The oil well head has been observed according to 3 viewpoints, showing the simulator flexibility. On the second scene, two wrecks can be observed on the slope of a basin along with small patches of rocks. These features are consistent with real Klein sidescan sonar acquisitions on the same area [3] and also appear on the simulated multibeam echosounder data.

2) Simulating multibeam echosounders:

a) Aggregation principles: Each Rx beam from the multibeam echosounder, is described by a specific Rx sector which is split into Rx elementary tubes according to the same process as previously. A series of energy contribution along time is then computed for each Rx beam. Based on amplitude detection, the first temporal return among these contributions, provides the beam sounding characterizing the return time travel between the sensor and the intersected scene.

b) Results: A RESON 8101 survey has been simulated on the second reference scene (Sydney sea-bottom). On the collected data, the two wrecks observed on the simulated sidescan images are logically present along with some small rocks over the slopes of the basin.

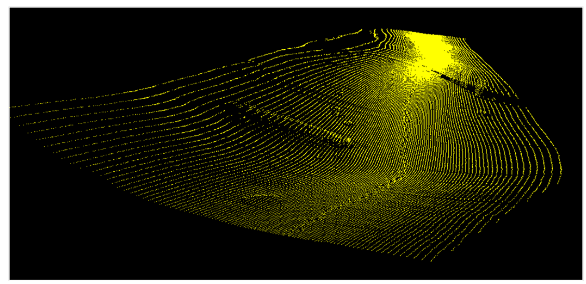

Fig. 5. Multibeam echosounder simulation on the sydney harbor scene

III. Introducing a new sensor : DIDSON front looking sonar

Based on high frequency sonar, DIDSON acoustic cameras provide high resolution images of underwater environments when optical systems get blind mainly due to water high turbidity. For absorption reasons involved by their high frequencies, these cameras often have a few meters range. However, their image refresh rate can be rather high providing several views of quite the same area, allowing various applications like identification, inspection, navigation or surveillance missions for either fauna studies [6][7] or more human security related activities [8][9].

A. Sensor description

1) Beamforming: DIDSON system uses acoustic lenses to perform direct and energy saving beamforming. Figure 6 shows how the backscattered acoustic waves are focused by the consecutive lenses (from L1 to L3) at specific locations on the antenna T according to their arrival angles. A L1 perpendicular wave will be focused at the location 0° on T, while differently oriented arriving waves will be aggregated at other locations on T.

The length of antenna T is split into 48 or 96 cells (or beams), each beam being 0.3° width with spacing ranging from 0.3° to 0.4°, for a full 29° azimuth coverage. Sampling along time the energy focused inside each cell provides per-beam backscattered signal according to range.

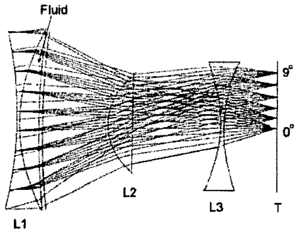

Fig. 6. DIDSON acoustic lenses beamforming [10]

2) Image construction: A DIDSON image gathers all the previous collected backscattered signal samples per beam and per range. However, according to the system frequency (high or low resolution), a full DIDSON image (48 or 96 beams) is built from the reverberation received by 4 or 8 sets of 12 non-adjacent beams fired simultaneously. Thus, this interlacing technique requires several Tx/Rx cycles to produce a complete image but aims at preventing beams cross-talk. Indeed, Figure 7 gives the acoustic beam pattern for three 2.6° spaced beams, showing that two neighboring (0.3° spaced) beams cannot be used within a single cycle.

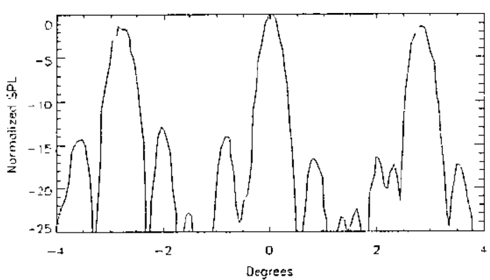

Fig. 7. DIDSON Tx and Rx acoustic patterns [10]

Nevertheless, depending on the shape and nature of the observed object, cross-talk phenomena are still observed on real images (see Figure 8) as side lobes may gather enough energy contributions from round-shaped objects that reflect transmitted energy to all directions.

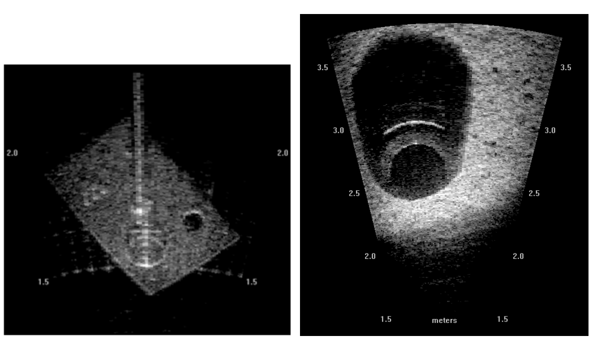

(a) Metal plate (b) Tire

Fig. 8. Example of real DIDSON images

After several cycles, the full image being built is stored as a frame within a DDF file that gathers all the frames from a survey.

B. DIDSON acoustic camera new component

The component in charge of simulating DIDSON acoustic camera needs to take into account the sensor Tx and Rx patterns to gather correctly the backscattered energy described through the lists of Rx elementary tubes. Moreover, according the considered cycle, only sectors corresponding to the fired beams are used for data collection.

1) Image simulations: A survey with the new DIDSON virtual camera has been simulated on each reference scene producing two DDF files. Figure 9 exhibits two frames extracted from the Sydney harbor DDF file, clearly showing the big wreck and the rocky patches, already displayed by both the previous sensors.

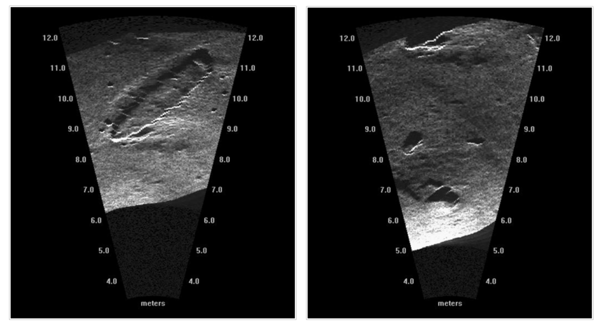

(a) Wreck (b) Small rocks

Fig. 9. Simulated sonar images extracted from a sequence produced on the Sydney area

Figure 15 proposes other examples of simulated images on the oil well head scene.

2) Observing cross-talk phenomenon: When performing simulation on round-shaped objects, cross-talk phenomena are observed the same way as with images coming from a real DIDSON camera.

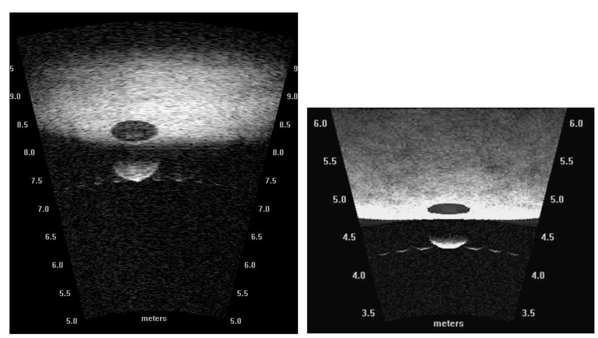

(a) Real (b) Simulated

Fig. 10. Real & simulated DIDSON images with crosstalk phenomenon on a sphere lying on a flat bottom

Figure 10 presents both real and simulated images on a scene containing a sphere lying on a flat bottom. Cross-talks are logically observed on both real and simulated images as round objects reflect the transmitted acoustic wave to all directions. Indeed, the backscattered signal is received through the side lobes of the fired beams according to Figure 7 actual sensor beam pattern provided by the acoustic lenses.

IV. Introducing georeferenced perturbation

Using facets or DTM cells for describing items inside an underwater scene defines the resolution of the geometrical features seen by the sensors during any simulation. However, many phenomena come from higher resolution scene features. For instance, on real DIDSON images collected in a flat bottom pool, some consistency or patterns between consecutive images are observed, besides the fluctuating noise. A cross-correlation between these images confirms the georeferenced characteristics of these patterns as shown in Figure 11 for a sequence acquired using a linear constant speed trajectory. The observed patterns clearly show that modeling a flat bottom by a flat DTM only, is not enough. Indeed, they reveal the bottom response occurs at a finer resolution than the one used for DTM description.

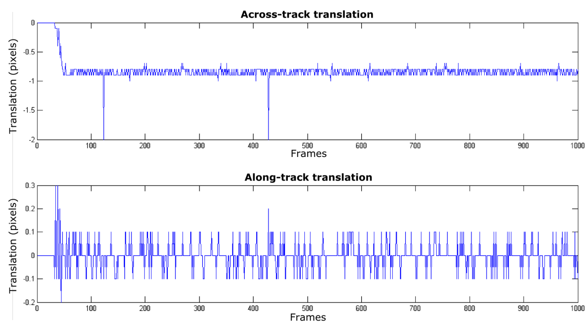

Fig. 11. Sensor trajectory analysis from cross-correlations between consecutive frames of the straight linepool survey

The next sections will present two approaches to allow a more detailed scene description, producing either *macro-textures* or *micro-textures*.

A. Macro-textures

This first approach introduces georeferenced perturbations to the elevation surface modeling the observed scene, by decomposing each facet into smaller ones (sub-facets). Adding the global elevation coming from the underlying facet (DTM or object) to a small variation produced by a local and finer elevation map, gives each sub-facet elevation. Each sub-facet will then produce a specific response giving a more realistic characterization of the encompassing facet.

Various techniques may produce adequate local elevation maps depending on the textures to be simulated. These textures clearly depend on the scene sea-bottom sedimentology. Rocky sea-bottoms may be obtained using standard fractal techniques like fractional Brownian motion [11]. Moreover, shifting fractional Brownian motion spectral components allows producing oriented textures; the direction and amplitude of the produced ripples depend on the direction and length of the spectral translation [12].

Figure 12 shows examples of simulated texture images using these techniques to produce local elevation maps. As these maps modify the scene elevation, they can introduce textures with shadow, in the simulated images. Moreover, these maps

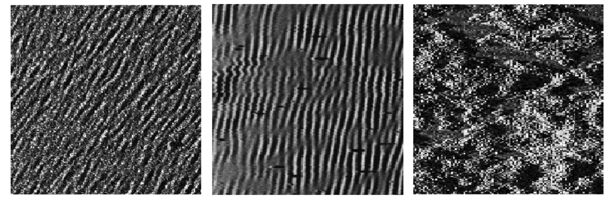

(a) Soft ripples (b) Sharp ripples (c) Rocky area

Fig. 12. Using macro-textures to simulate sea-bottom elevation features

can also be either offline or online computed, the latter offering reduced memory allocation and more flexibility for adapting the required level of resolution, but at extra computation costs.

Thus, without any modification of the simulator core, introducing local georeferenced perturbations to the global elevation map, allows producing more realistic sea-bottoms textures (with structured shadows) reflecting local seabed altitude variations.

B. Micro-textures

The second approach that produces *micro-textures* does not involve elevation perturbations but introduces georeferenced perturbations to the facet reflection properties. In that case, the standard backscattered energy transmitted by each Rx elementary tube is modulated by a local contribution linked to both the statistical properties of the facet (sedimentologic nature, material, . . .) and the location on this facet. Thus, modifying the backscattered energy at the elementary tube resolution allows tuning image granularity inside facets. However, unlike the macro-texture approach, this micro-texture approach cannot produce textures with shadows.

Figure 13 illustrates the impact of such georeferenced backscattering modifications on simulated images with various micro-textures corresponding to several sandy sea-bottoms.

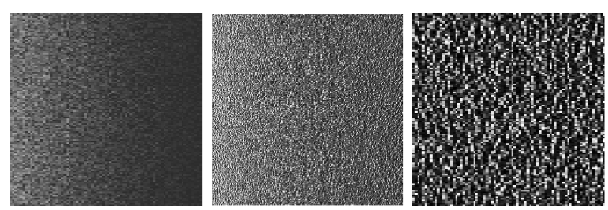

(a) Mud (b) Sand (c) Gravel

Fig. 13. Using micro-textures to simulate various kind of sandy sea-bottoms

As for macro-textures, micro-textures can be generated either though pre-computed maps or online during the simulation through georeferenced perturbation functions. The underlying micro-texture used for the next simulation results has been generated online using Perlin noise [13] and counted for 25% of the diffuse reflection component.

C. Simulation results

As previously mentioned, consecutive DIDSON frames exhibit a meaningful level of correlation between images. Micro-textures, being georeferenced by definition, induce such cross-correlations between simulated images computed on the same scene area, involving results similar to Figure 11. Figure 14 illustrates such correlations on several consecutives images extracted from a sequence simulated with a flat sea-bottom with a straight constant speed trajectory. The yellow dotted circle outlines a visible pattern between the three frames. As the sensor moves along its trajectory, the pattern slowly drifts towards the sensor water column (first return recorded by the sensor).

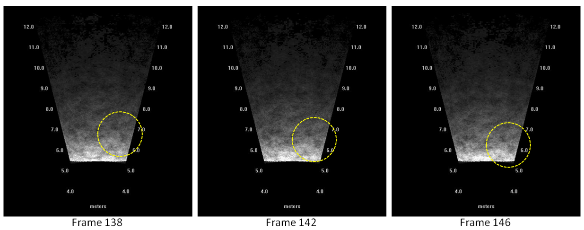

Fig. 14. Neighboring frames (with consistent micro-textures) extracted from a simulated DIDSON sequence with a straight constant speed sensor trajectory

Finally, Figure 15 compares two simulations performed with the oil well head scene. As the sea-bottom from the left image is only modeled by a flat DTM with no micro-textures, no structured pattern appears: the backscattered energy is only affected by random and uncorrelated noise. On the contrary, the right image integrates georeferenced perturbations in the reflection: the underlying flat bottom produces uneven intensities across the image. Moreover, as micro-textures adds spatially structured contributions to the basic backscattering, some smoothing effect is also observed.

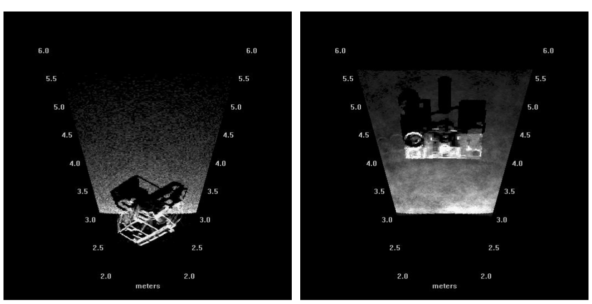

(a) No cross-talk, no micro-texture

(b) Cross-talk, micro-texture

Fig. 15. DIDSON simulated images and georeferenced perturbations using Perlin noise

V. Conclusion & Perspectives

A highly modular sonar simulation framework has been presented in this paper. All the simulated images, computed in various tailored environments, show the efficiency of such a framework in terms of scene description capabilities and computational engine choices. Moreover, this paper validates the extensibility of our simulation framework design for integrating new sensors with their specificities while keeping generic propagation engine behaviors. Indeed, a specific DIDSON virtual acoustic camera has been introduced, producing realistic front looking sonar images, without any modification of the engine cores.

Producing realistic output for a simulator strongly depends on the resolution of the scene description. Indeed, the scene model may not provide resoluted enough description due to a limited DTM resolution or roughly facet-described objects. In that case, when extra knowledge is available about the scene nature, this paper introduces the ability to use synthetic features in order to bypass the scene resolution and provide realistic images with parameters corresponding to reality. On the top of the scene description, georeferenced perturbations have been added allowing finer texture simulations by modifying locally either over-sampled local elevation maps (macro-textures) or tube backscattered energies.

These new georeferenced perturbations successfully permit more realistic outputs. Indeed, being georeferenced and adaptive (online generation), these perturbations may characterize the sea-bottom behavior at a very precise scale allowing to take into account any complex and finer phenomenon. Thus, they also participate in an on-going effort, with adequate modeling, to simulate full sonar signals by dealing with sub-facet resolution behaviors (for instance, the decorrelation between sensors when simulating interferometric signals, . . .).

References

[1] D. Alexandrou, "Computer simulations of bathymetric sidescan sonar," in *OCEANS 87 : The Ocean - An international workplace*, vol. 19, Sep. 1987, pp. 1168–1173.

[2] D. Guériot, S. Daniel, and E. P. Maillard, "Sonar images and swath bathymetry simulations for environment restitution through acoustical ray tracing techniques," in *Fourth European Conference on Underwater Acoustics*, vol. 1, Rome, Italy, September 1998, pp. 425–431.

[3] D. Gueriot, C. Sintes, and R. Garello, "Sonar data simulation based on tube tracing," in *OCEANS 2007 - Europe*, 18-21 June 2007, pp. 1–6.

[4] D. Australia Defense Science & Technology Organization, "Common data set," in *Shallow Survey 99 - International Conference on High Resolution Surveys in Shallow Water*, Sydney, Australia, Oct. 1999.

[5] D. Guériot, J. Chèdru, S. Daniel, and E. Maillard, "The patch test: a comprehensive calibration tool for multibeam echosounders," in *OCEANS 2000 MTS/IEEE Conference and Exhibition*, vol. 3, Providence, Rhode Island, USA, Sep. 2000, pp. 1655–1661.

[6] J. A. Holmes, G. M. Cronkite, H. J. Enzenhofer, and T. J. Mulligan, "Accuracy and precision of fish-count data from a "dual-frequency identification sonar" (DIDSON) imaging system," *ICES J. Mar. Sci.*, vol. 63, no. 3, pp. 543–555, 2006.

[7] R. P. Mueller, R. S. Brown, H. Hop, and L. Moulton, "Video and acoustic camera techniques for studying fish under ice: a review and comparison," *Reviews in Fish Biology and Fisheries*, vol. 16, no. 2, pp. 213–226, May 2006.

[8] A. Asada, F. Maeda, K. Kuramoto, Y. Kawashima, M. Nanri, and K. Hantani, "Advanced surveillance technology for underwater security sonar systems," *OCEANS 2007 - Europe*, pp. 1–5, 18-21 June 2007.

[9] E. Belcher, B. Matsuyama, and G. Trimble, "Object identification with acoustic lenses," *OCEANS, 2001. MTS/IEEE Conference and Exhibition*, vol. 1, pp. 6–11 vol.1, 2001.

[10] E. Belcher, W. Hanot, and J. Burch, "Dual-frequency identification sonar DIDSON," *Underwater Technology, 2002. Proceedings of the 2002 International Symposium on*, pp. 187–192, 2002.

[11] A. P. Pentland, "Fractal-based description of natural scenes," *Pattern Analysis and Machine Intelligence, IEEE Transactions on*, vol. PAMI-6, no. 6, pp. 661 –674, nov. 1984.

[12] S. Guillaudeux and E. Maillard, "Seabed simulations with fractal techniques," vol. 1, sep-1 oct 1998, pp. 433 –437 vol.1.

[13] K. Perlin, "Improving noise," in *SIGGRAPH '02: Proceedings of the 29th annual conference on Computer graphics and interactive techniques*. New York, NY, USA: ACM, 2002, pp. 681–682.